

## Optical QPOs with 550 day periodicity in the reverberation mapped broad line quasar PG 1411+442

XUE-GUANG ZHANG<sup>1</sup>

<sup>1</sup>Guangxi Key Laboratory for Relativistic Astrophysics, School of Physical Science and Technology, GuangXi University, Nanning, 530004, P. R. China

Submitted to ApJ

### ABSTRACT

In this manuscript, optical quasi-periodic oscillations (QPOs) with 550 day periodicity related to a candidate of sub-pc binary black hole (BBH) system are reported in the reverberation mapped broad line quasar PG 1411+442 but with different line profile of broad H $\alpha$  from that of broad H $\beta$  in its rms spectrum. First, considering sine function to describe the 18.8years-long light curves from the CSS, ASAS-SN and ZTF, 550days periodicity can be confirmed with confidence level higher than  $5\sigma$ . Second, the stable 550days optical QPOs can be re-confirmed with confidence levels higher than  $5\sigma$  by the Generalized Lomb-Scargle periodogram, the sine-like phase-folded light curves and the WWZ technique determined power maps. Third, based on simulated light curves by CAR process, confidence level higher than  $3.5\sigma$  can be confirmed for the optical QPOs not related to intrinsic AGN variability. Moreover, considering spatial separation of central two BH accreting systems smaller than expected sizes of broad emission line regions (BLRs), central total BH mass higher than  $10^6 M_{\odot}$  could lead to few effects of supposed BBH systems on estimated virial BH masses. Meanwhile, disk precession is not preferred due to the similar estimated sizes of optical and NUV emission regions, and jet precession can be ruled out due to PG 1411+442 as a radio quiet quasar. The results strongly indicate it would be practicable by applying very different line profiles of broad Balmer emission lines to detect candidates of BBH systems in normal broad line AGN in the near future.

*Keywords:* galaxies:active - galaxies:nuclei - quasars:emission lines - quasars: supermassive black holes

### 1. INTRODUCTION

Sub-pc binary black hole (BBH) systems are natural products in central regions of galaxies after considering galaxy merging as an essential process of hierarchical galaxy formation and evolution, as well discussed in Begelman et al. (1980); Silk & Rees (1998); Mayer et al. (2010); Fragione et al. (2019); Mannerkoski et al. (2022); Wang et al. (2023); Attard et al. (2024). In order to identify candidates of sub-pc BBH systems, the long-standing optical Quasi-Periodic Oscillations (QPOs) with periodicities around hundreds to thousands of days are accepted as one of the preferred indicators. Here, some of the known optical QPOs related to candidates of sub-pc BBH systems are listed. Graham et al. (2015a); Liu et al. (2018); Kovacevic et al. (2019) have reported reliable 1800days optical QPOs in the known quasar PG 1302-102, through its combined light curves covering more than 4 cycles.

Liu et al. (2015) have reported 540days optical QPOs in PSO J334.2028+01.4075, through its combined light curves covering more than 5 cycles. Graham et al. (2015); Charisi et al. (2016) have reported two samples of more than 160 optical QPOs with different periodicities, through the light curves covering at least 1.5 cycles. Zheng et al. (2016) have reported 1500days optical QPOs in SDSS J0159, through its light curve covering around 2 cycles. Serafinelli et al. (2020) have reported 1150days optical QPOs in Mrk915, through its light curve covering 3 cycles. Kovacevic et al. (2020) have reported 1.2yr optical QPOs in Mrk231, through its light curve covering more than 10 cycles. Liao et al. (2021) have reported 1607days optical QPOs in SDSS J0252, through its combined light curve covering more than 4 cycles. Zhang (2022a,b, 2023a) have reported 6.4yr optical QPOs in SDSS J0752 and 3.8yr optical QPOs in SDSS J1321 and 340days optical QPOs in SDSS J1609, through their light curves covering more than 2 cycles, 4 cycles and 4.5 cycles, respectively.

Besides optical QPOs, different line profiles of broad Balmer emission lines can also be applied to identify candidates for sub-pc BBH systems in broad line AGN. We

Zhang (2021) have firstly shown the very different line profiles of broad Balmer lines accepted as an indicator of a central BBH system in SDSS J1547 with double-peaked broad  $H\beta$  but single-peaked broad  $H\alpha$ . Meanwhile, 2159days optical QPOs can be confirmed in SDSS J1547 as shown in Zhang (2021). More recently, we Zhang (2023b) have shown that different line profiles of broad Balmer emission lines can be expected to have very different line width ratios from standard values, considering different effects of orbital obscuration on the two independent BLRs (broad emission line regions) related to the central sub-pc BBH systems in normal broad line AGN. And in Zhang (2023b), we have shown the 1000days optical QPOs in the broad line AGN SDSS J1257 with the line width ratio 0.69 of broad  $H\beta$  to broad  $H\alpha$  very different from the standard value 1.1 for normal quasars as discussed in Greene & Ho (2005). Applications of different line profiles of broad Balmer emission lines to identify candidates for BBH systems can avoid effects of short time durations on reliability of optical QPOs, if only though optical QPOs to identify BBH systems.

In the current stage, it is our research project to detect and identify more candidates for BBH systems in normal broad line AGN but with different line profiles of broad Balmer emission lines. Therefore, we start our research work among the known reverberation mapped broad line AGN with public spectroscopic results on broad emission lines. Among the reverberation mapped broad line AGN in Peterson et al. (2004), considering the measured line widths and the corresponding uncertainties, PG 1411+442 has unique properties of the varying components in broad Balmer emission lines in its rms spectrum (removing effects of none-variability components). Its broad  $H\alpha$  has second moment  $2437 \pm 196\text{km/s}$  to be about  $1.52^{+0.32}_{-0.25}$  times of second moment  $1607 \pm 169\text{km/s}$  of broad  $H\beta$ , however the broad  $H\alpha$  has full width at half maximum (FWHM)  $1877 \pm 375\text{km/s}$  to be about  $0.78^{+0.32}_{-0.23}$  times of FWHM  $2398 \pm 353\text{km/s}$  of the broad  $H\beta$ . The very different line width ratios strongly indicate very different line profile of the varying component in the broad  $H\alpha$  from that in the broad  $H\beta$  in the rms spectrum of PG 1411+442. Therefore, it is interesting to check long-term variability properties of PG 1411+442, to determine expected optical QPOs, motivated by its very different line profiles of the varying components in the broad Balmer emission lines in its rms spectrum, which is the main objective of this manuscript. Section 2 presents main results on the long-term optical variability of PG 1411+442. Section 3 shows the necessary discussions. Section 4 gives final summary and main conclusions. In this manuscript, the cosmological parameters have been adopted as  $H_0 = 70\text{km} \cdot \text{s}^{-1}\text{Mpc}^{-1}$ ,  $\Omega_\Lambda = 0.7$  and  $\Omega_m = 0.3$ .

## 2. OPTICAL QPOS IN PG 1411+442

PG 1411+442 at  $z \sim 0.0896$  is a known reverberation mapped broad line AGN discussed in Kaspi et al. (2000); Peterson et al. (2004). The 18.8years-long light curves of PG 1411+442 shown in Fig. 1 can be collected from the Catalina Sky Survey (CSS) (Drake et al. 2009) with MJD-53000 from 509.35 (May, 2005) to 3462.28 (June, 2013), from the All-Sky Automated Survey for Supernovae (ASAS-SN) (Shappee et al. 2014; Kochanek et al. 2017) with MJD-53000 from 2985.10 (March, 2013) to 7374.81 (March, 2024), from the Zwicky Transient Facility (ZTF) (Bellm et al. 2019; Dekany et al. 2020) with MJD-53000 from 5202.37 (March, 2018) to 7194.16 (September, 2023). Then, similar as what we have recently done in Zhang (2023a), the following four methods are applied to check whether are there optical QPOs in PG 1411+442.

For the first method (the direct-fitting method), a 8th-degree polynomial function plus a sine component with periodicity  $T_q$  are applied to describe each light curve  $LC_{k,t}$  from the different sky survey projects,

$$LC_{k,t} = \sum_{i=0}^8 (a_{k,i} \times t_k^i) + g_k \times \sin\left(\frac{2\pi t_k}{T_q} + \phi_{0,k}\right) \quad (1)$$

, with the suffix  $k$  meaning which light curve (CSS V-band, ASAS-SN V-band, ASAS-SN g-band, ZTF g-band, ZTF r-band, ZTF i-band) is used, and the parameters  $a_{k,i}$  as the polynomial coefficients. When the six light curves are being simultaneously described by the model functions above, the parameters  $a_{k,i}$ ,  $g_k$  and  $\phi_{0,k}$  are different but  $T_q$  are fixed for the light curves from the different sky survey projects. Then, through the Levenberg-Marquardt least-squares minimization technique (the known MPFIT package) (Markwardt 2009), the best descriptions and the corresponding residuals (the light curves minus the best descriptions) can be determined and shown in Fig. 1 with  $\chi^2/dof \sim 2.39$  ( $dof$  as the degree of freedom). The determined periodicity and the corresponding  $1\sigma$  uncertainty are  $550 \pm 2\text{days}$ . Although the  $\chi^2/dof \sim 2.39$  is larger than 1, the determined fitting results can be accepted, mainly due to the following main reason. The collected light curves are not smooth enough but with some sharp features (probably related to intrinsic AGN variability), therefore the applied polynomial component plus sine components cannot lead to the determined fitting results with  $\chi^2/dof \sim 1$ . In top panel of Fig. 1, four apparently sharp features in the light curves are marked by vertical dashed lines in dark red. Moreover, as a comparison, two light curves from CSS are collected for the SDSS J080648.65+184037.0 and MS 10548-0335 reported in the sample of Graham et al. (2015) to have robust QPOs with periodicities around 890days. Based on a 8th-degree polynomial component plus a sine component, the best descriptions to the two light curves are shown in Fig. 2, with the determined  $\chi^2/dof$  about 2.5 in SDSS J080648.65+184037.0 but

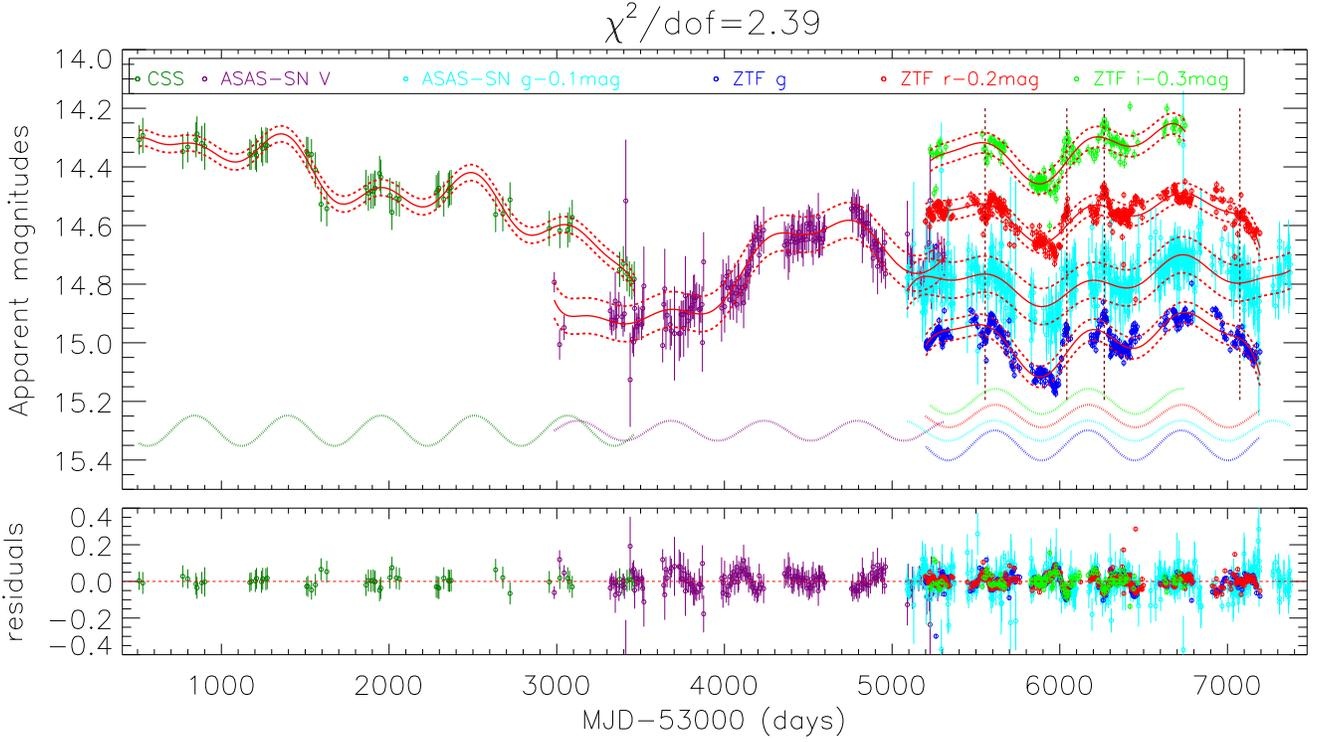


**Figure 1.** Top panel shows the 18.8years-long light curves (open circles plus error bars) and the best descriptions (solid red lines) and the corresponding 1RMS scatters (dashed red lines) by the sine function plus trends described by 8th-degree polynomial functions. As shown in the legend, open circles in dark green, in purple, in cyan, in blue, in red and in green show the collected 1day binned data points from the CSS, the ASAS-SN V-band, the ASAS-SN g-band (minus 0.1mag), the ZTF g-band, the ZTF r-band (minus 0.2mag) and the ZTF i-band (minus 0.3mag), respectively. The dotted line in different color in bottom region of the top panel shows the determined sine component in the light curve shown as the same color. The vertical dashed lines in dark red mark four apparently sharp features in the light curves. Bottom panel shows the residuals calculated by the light curves minus the best descriptions, with horizontal dashed red line as the residuals equal to zero.

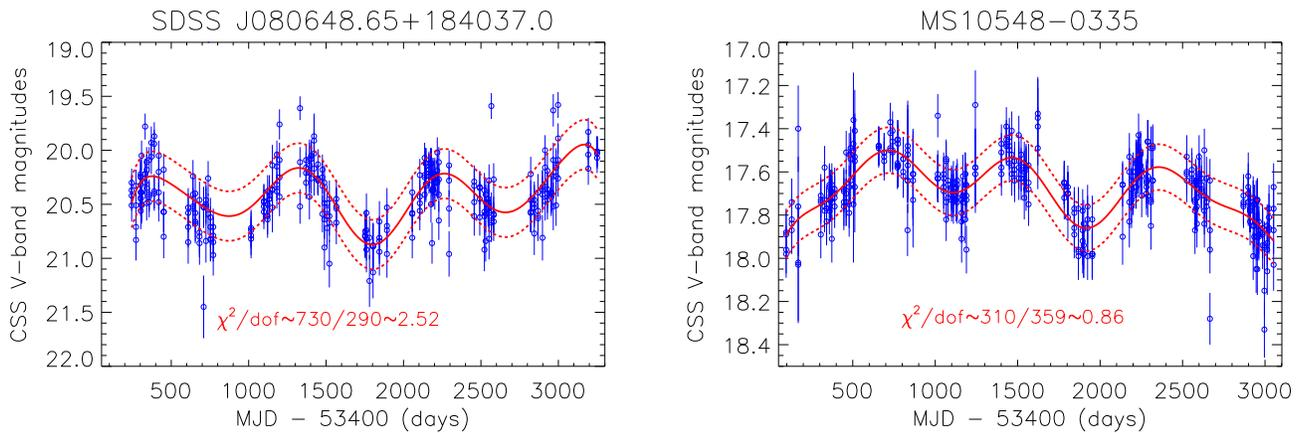


**Figure 2.** Best fitting results and the corresponding  $\chi^2/dof$  to the light curves of SDSS J080648.65+184037.0 and MS 10548-0335 with reported QPOs in Graham et al. (2015). In each panel, open circles plus error bars in blue show the light curve from the CSS, solid red line and dashed red lines show the best descriptions and the corresponding 1RMS scatters by the sine function plus a 8th-degree polynomial trend.

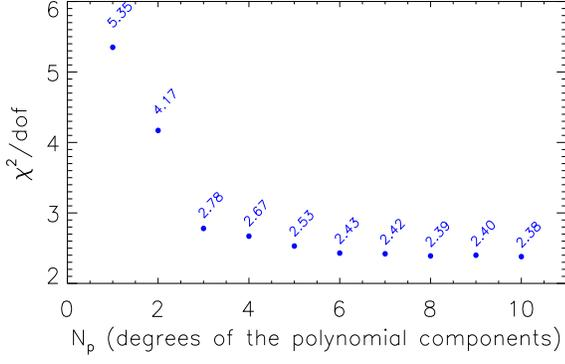


**Figure 3.** On the dependence of  $\chi^2/dof$  on different degrees for the polynomial components. Clear information of  $\chi^2/dof$  has been marked around each data point.

about 0.86 in MS 10548-0335. Therefore, although the determined fitting results lead  $\chi^2/dof$  to be apparently larger than 1, the shown fitting results in Fig. 1 can be reasonably accepted.

Here, in order to determine the degree of the applied polynomial components, different degrees  $N_p$  have been applied, leading to the corresponding values  $\chi^2/dof$ . As shown in Fig. 3 for the dependence of  $\chi^2/dof$  on  $N_p$ , there are none apparent variability of  $\chi^2/dof$  for  $N_p \geq 8$ . Therefore, the 8th degree polynomial components are accepted. Furthermore, besides the 8th-degree polynomial functions plus sine components, a 30th-degree polynomial functions without considering any sine components applied to describe the light curves can lead to the  $\chi^2/dof \sim 2.5$  related to the new model polynomial functions. Then, through the F-test technique as what we have recently done in Zhang (2023a), the sine components are preferred with confidence levels higher than  $7\sigma$ , rather than pure applications of higher degree polynomial functions.

For the second method, after subtracting the trends described by the 8th-degree polynomial functions, the corresponding phase-folded light curves with accepted the determined periodicity  $550 \pm 40$ days are shown in Fig. 4, which can be described by the sine function  $\sin(2\pi t + \phi_0)$ . As an extension of the directing fitting method, application of the phase-folded method can show QPOs more intuitively in phase space, to support the optical QPOs in the light curves of PG 1411+442.

For the third method, the widely accepted Generalized Lomb-Scargle (GLS) periodogram (Lomb 1976; Scargle 1982; Zechmeister & Kurster 2009; VanderPlas 2018) (python package of astroML.time\_series, [https://www.astroml.org/\\_modules/astroML/time\\_series/periodogram.html#lomb\\_scargle](https://www.astroml.org/_modules/astroML/time_series/periodogram.html#lomb_scargle)) is applied to the light curves after subtractions of the polynomial trends. Here, due to small number of data points in the CSS light curve and short time duration of the ZTF

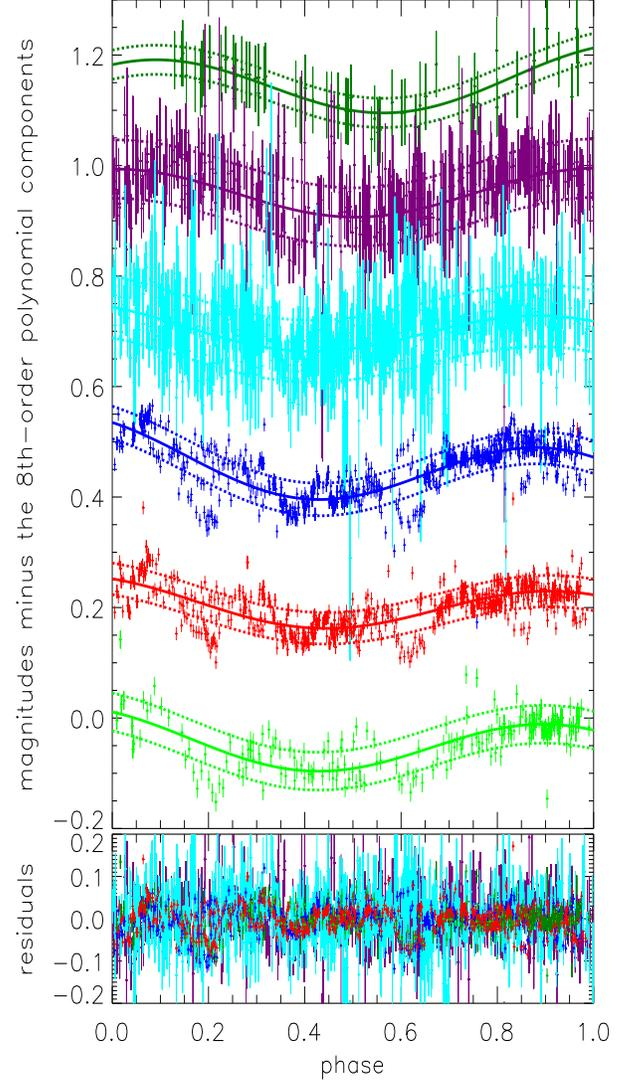


**Figure 4.** Top panel shows the phase folded light curves (crosses plus error bars in different colors) after removing the polynomial trends and the best descriptions (solid lines in different colors) and the corresponding 1RMS scatters (dashed lines in different colors) by the sine function. In top panel, symbols and line styles in dark green, in purple, in cyan, in blue, in red and in green show the corresponding results for the light curves from the CSS (plus 1.15mag), ASAS-SN V-band (plus 0.95mag), ASAS-SN g-band (plus 0.7mag), and ZTF g/r/i-band (plus 0.45mag, plus 0.2mag, minus 0.05mag), respectively. Bottom panel shows the corresponding residuals (in the same color) calculated by the folded light curve minus the best descriptions.

i-band light curve, the GLS periodogram is not applied to the CSS light curve nor to the ZTF i-band light curve. Top panel of Fig. 5 shows the GLS power properties. It is clear for the periodicity around 500-600days with confidence level higher than  $5\sigma$  (the false-alarm probability of  $5e-7$ ) determined by the bootstrap method as discussed in Ivezić et al.

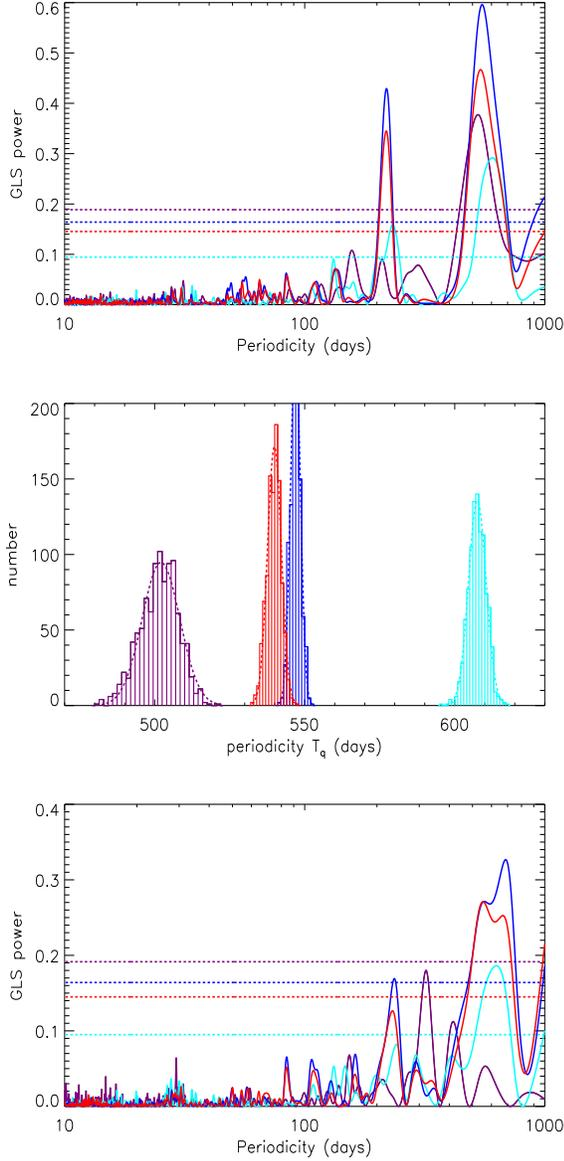


**Figure 5.** Top panel shows the power properties through the Generalized Lomb-Scargle periodogram. In top panel, solid line in purple, in cyan, in blue and in red represent the results through the ASAS-SN V-band line curve, ASAS-SN g-band light curve, ZTF g/r-band light curves, after removing the polynomial trends. The corresponding  $5\sigma$  confidence level is shown as the horizontal dashed line in the same color. Middle panel shows the distributions of GLS determined periodicities through the bootstrap method. In middle panel, histogram in purple, in cyan, in blue and in red show the corresponding results through the ASAS-SN V-band line curve, ASAS-SN g-band light curve, ZTF g/r-band light curves. And the thick dashed line in the same color shows the Gaussian described results to the corresponding distribution. Bottom panel shows the power properties through the light curves without subtractions of any polynomial trends. In bottom panel, line styles have the same meanings as those in the top panel.

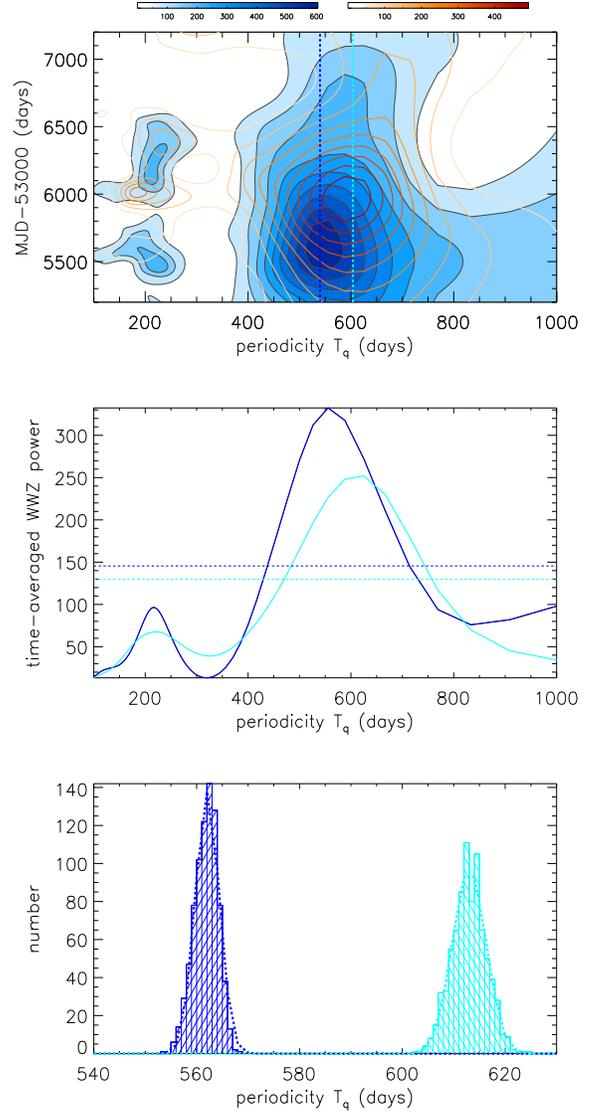


**Figure 6.** Top panel shows the two dimensional power maps determined by the WWZ method. Middle panel shows the WWZ method determined time-averaged power properties. Bottom panel shows the bootstrap method determined periodicity distributions. In top panel, the vertical dashed lines mark the WWZ method determined periodicities, contour filled with bluish colors represent the results through the ZTF g-band light curve after removing the polynomial trend, contour with levels shown in reddish colors represent the results through the ASAS-SN g-band light curve after removing the polynomial trend. In top regions of top panel, color bars show the corresponding number densities for the contour levels. In middle panel, the horizontal dashed blue line and horizontal dashed purple line mark the corresponding  $5\sigma$  confidence levels for the periodicities through the Monte Carlo method. In bottom panel, histogram filled by blue lines and filled by purple lines show the WWZ determined periodicity distributions by the bootstrap, through the ZTF g-band and ASAS-SN g-band light cures after removing the polynomial trends, respectively, and thick dashed line in the same color shows the Gaussian described results to the corresponding distribution.

(2019). Meanwhile, as shown in the middle panel of Fig. 5, the well-known bootstrap method within 1000 loops is applied to determine the periodicities and the corresponding uncertainties about  $502\pm 7$ days,  $607\pm 3$ days,  $547\pm 2$ days and  $540\pm 2$ days for the ASAS-SN V-band, the ASAS-SN g-band and the ZTF g/r-band light curves, respectively.

Before proceeding further, two additional points are noted. First, through the collected light curves from different sky survey projects, the determined periodicities by the GLS periodogram (also by the following WWZ technique) are a bit different, probably due to effects of intrinsic AGN variability. More detailed discussions on the effects of AGN variability on the determined periodicities related to sub-pc BBHs systems will be given in one manuscript which we have submitted to ApJ. Second, the GLS periodogram is also applied to the collected ZTF g/r-band light curves and ASAS-SN V/g-band light curve, without subtractions of any polynomial trends from the light curves. The results can be applied to confirm that the subtractions of polynomial trends have few effects on our determined periodicities but can lead to more apparent signs for QPOs. The corresponding GLS power properties are shown in the bottom panel of Fig. 5. It is clear that apparent peaks around 500-600days with confidence level higher than  $5\sigma$  can be confirmed in the GLS power properties through the ZTF g/r-band and ASAS-SN g-band light curves. However, there is no reliable periodicity with confidence level higher than  $5\sigma$  in the GLS power properties through the ASAS-SN V-band light curve. Therefore, the applied polynomial trends lead to the same but more significant peaks in the GLS power properties through the light curves.

For the fourth method, the WWZ (Weighted wavelet z-transform) technique (Foster 1996; An et al. 2016; Gupta et al. 2018; Kushwaha et al. 2020; Li et al. 2021) (the python code `wwz.py` written by M. Emre Aydin, <https://github.com/eaydin/WWZ/blob/master/wwz.py>) is applied to check the optical periodicities in PG 1411+442 with frequency step of 0.0001 and searching periodicities from 100 days to 1000 days. The corresponding results are shown in Fig. 6 with  $5\sigma$  confidence levels determined by common Monte Carlo method applied through 3.2 million randomly created light curves by white noise process. Here, due to small number of data points in the CSS light curve and large time gaps in the ASAS-V band light curve and short time duration of the ZTF i-band light curve, the WWZ technique is not applied to the CSS, ASAS-V band and ZTF i-band light curves. Meanwhile, due to totally similar WWZ determined results for the ZTF g-band light curve and the ZTF r-band light curve, only the WWZ determined results for the ZTF g-band light curve are shown in Fig. 6. Clearly similar periodicities around  $562\pm 3$ days in the ZTF g/r-band light curves and  $613\pm 3$ days in the ASAS-SN g-band light curve can be

confirmed as shown in the bottom panel of Fig. 6 through the bootstrap method.

Therefore, the optical QPOs with periodicities around 500-600days (mean value and uncertainty as  $\sim 550\pm 50$ days) in PG 1411+442 can be detected from the 18.8years-long light curves (time duration about 12.5 times longer than the detected periodicities) with confidence level higher than  $5\sigma$ , based on the best-fitting results directly by the sine function shown in Fig. 1, on the sine-like phase-folded light curve shown in Fig. 4, on the results of GLS periodogram shown in Fig. 5, and on the results determined by the WWZ technique shown in Fig. 6.

Furthermore, the similar procedure as recently done in Zhang (2023a) and also similar as done in Vaughan et al. (2016) is applied to test whether the optical QPOs were actually related to intrinsic AGN variability of PG 1411+442. Based on the CAR (the first order Continuous AutoRegressive) process in Kelly, Bechtold & Siemiginowska (2009),

$$dLC_t = \frac{-1}{\tau} LC_t dt + \sigma_* \sqrt{dt} \epsilon(t) + LC_0 \quad (2)$$

with  $\epsilon(t)$  as a white noise process with zero mean and variance equal to 1,  $16660/(1-(1-P_4)^{16660})$  with  $P_4$  as the  $4\sigma$  probability) light curves  $LC_t$  with the same time information of CSS, ASAS-SN V-band and ASAS-SN g-band light curves as shown in Fig. 1 are created, with variability timescale  $\tau/\text{days}$  randomly selected from 50days to 1000days and variability amplitude  $\sigma_*/(\text{mag}/\text{day}^{0.5})$  randomly selected from  $0.006\text{mag}/\text{day}^{0.5}$  to  $0.03\text{mag}/\text{day}^{0.5}$ , with the timescales and amplitudes being the common values for normal quasars as shown in Kelly, Bechtold & Siemiginowska (2009); Kozłowski et al. (2010); MacLeod et al. (2010) and with  $LC_0 = 14.83$  (the mean magnitude of the combined CSS, ASAS-SN V-band and ASAS-SN g-band light curves). Then, among the 16660 light curves, there are only 8 light curves with probably QPOs with periodicities around  $550\pm 100$ days, detected by the GLS method with confidence levels higher than  $5\sigma$  and determined by the Equation (1) leading to the corresponding  $\chi^2/\text{dof} < 3$ . Therefore, the probability is lower than  $4.8 \times 10^{-4}$  ( $8/16660$ ) to detect fake QPOs through intrinsic AGN variability. In other words, the confidence level higher than  $3.5\sigma$  can be confirmed that the detected optical QPOs in PG 1411+442 are not related to intrinsic AGN variability.

Here, the first order CAR process is applied above. However, as discussed in Kelly et al. (2014); Kasliwal et al. (2017); Moreno et al. (2019); Yu et al. (2022); Kishore et al. (2024), higher order CARMA(p, q) ( $p \geq 1$  and  $q \leq p$ ) (Continuous AutoRegressive Moving Average) process rather than the simple first order CAR process (=CARMA(1,0)) should be possibly preferred to describe AGN variability. Meanwhile, the CARMA(p, q) process has been applied to test robustness of detected QPOs, such as the discussions

in Bhattacharyya et al. (2020); Tarnopolski et al. (2003). Therefore, it is necessary to check whether higher order CARMA(p, q) is preferred than the applied first order CAR process in the PG 1411+442. Based on the linear interpretation applied to the high quality ZTF g-band light curve of PG 1411+442, an evenly sampled light curve can be created with the same number of data points as that of the ZTF g-band light curve. Then, through both the Bayesian Information Criterion (BIC) and the Akaike Information Criterion (AIC), the orders (p=1, q=0) of the CARMA(p, q) process for the evenly sampled light curve can be determined through applications of the function arma\_order\_select\_ic in python package statsmodels ([https://tedboy.github.io/statsmodels\\_doc/doc/generated/statsmodels.tools.arma\\_order\\_select\\_ic.html](https://tedboy.github.io/statsmodels_doc/doc/generated/statsmodels.tools.arma_order_select_ic.html)). Therefore, it is efficient enough for applications of the CAR process to trace intrinsic AGN variability in PG 1411+442.

Before ending the section, two additional points should be noted. For the first point, as shown in Fig. 1, there really are large time gaps in the CSS light curve, therefore only the direct-fitting method is applied to the CSS light. The best fitting results with the same periodicity not only to the CSS light curve but also to the light curves from the other sky survey projects actually provide more stable evidence to support the optical QPOs in PG 1411+442, through the direct-fitting method. For the second point, as shown in Fig. 4, there are not the same quality for the folded light curves. However, considering different intrinsic AGN variability properties in different epochs and also the different time gaps in different light curves, the results in Fig. 4 can be reasonably accepted.

### 3. MAIN DISCUSSIONS

We firstly discuss whether an expected BBH system has effects on estimations of virial BH mass of reverberation mapped broad line AGN, which will provide further clues on the conditions that broad emission line properties can be applied to estimate total BH mass of a broad line AGN even harboring a BBH system.

Based on the optical QPOs with periodicity about 550days in PG 1411+442, assumed a BBH system as discussed in Eracleous et al. (2012), the expected space separation of the central BBH system in PG 1411+442 can be estimated as

$$S_{BBH} \sim 0.432M_8 \left( \frac{T_q/\text{year}}{2652M_8} \right)^{2/3} pc \sim 5.8_{-2.8}^{+4.8} \text{light - days} \quad (3)$$

with  $M_8$  as the BH mass in units of  $10^8 M_\odot$  and with the accepted virial BH mass  $(4.43 \pm 1.46) \times 10^8 M_\odot$  reported in Peterson et al. (2004). If only the space separation is very smaller than BLRs (broad emission line regions) in the central region of PG 1411+442, the dynamical properties of broad emission lines can be efficiently applied to determine total virial mass of central binary system. Considering the sizes of BLRs about 70-120 light-days of PG 1411+442 in Peterson et al. (2004) at least 10 times larger than the  $S_{BBH}$

in PG 1411+442, therefore, the estimated virial BH mass is efficient enough, simply accepted the two BLRs have been at least partly mixed similar as discussed in Shen & Loeb (2010).

Furthermore, simply considering the dependence of BH mass on continuum luminosity reported in Peterson et al. (2004) and the dependence of BLRs sizes  $R_{BLRs}$  on continuum luminosity reported in Kaspi et al. (2000); Bentz et al. (2013), the following formula can be found

$$\log(M_8) = -0.12 + 0.79 \times \log\left(\frac{L_{con}}{10^{44}}\right) \quad (4)$$

. In order to find  $S_{BBH} \approx R_{BLRs}$ , we will have

$$\log(M_8) \approx 1.89 \log\left(\frac{T_q}{\text{year}}\right) - 3.43 \quad (5)$$

. Simply considered  $M_{BH} \sim 10^8, 10^7, 10^6 M_\odot$ , we will have  $T_q \sim 220\text{years}, 19\text{years}, 5.7\text{years}$ . In one word, unless central total BH masses were around  $10^6 M_\odot$  or smaller leading to the expected  $S_{BBH}$  larger than  $R_{BLRs}$ , central BBH systems have few effects on estimations of virial total masses of central BHs.

We secondly discuss the other explanations to the optical QPOs in PG 1411+442, besides the assumed central BBH system.

The precessions of emission regions with probable hot spots for the optical emissions can also be applied to describe the detected optical QPOs in PG 1411+442. As discussed in Eracleous et al. (1995); Storchi-Bergmann et al. (2003), the expected disk precession period can be estimated as

$$T_{pre} \sim 1040M_8 R_3^{2.5} \text{yr} \quad (6)$$

, with  $R_3$  as distance of optical emission regions to central BH in units of 1000 Schwarzschild radii ( $R_g$ ). Considering the optical periodicity about 550days and the BH mass about  $(4.43 \pm 1.46) \times 10^8 M_\odot$ , the expected  $R_3$  could be around 0.04 in PG 1411+442. However, based on the discussed distance of NUV emission regions to central BHs in Morgan et al. (2010) through the microlensing variability properties of eleven gravitationally lensed quasars, the NUV 2500Å continuum emission regions in PG 1411+442 have distance from central BH as

$$\log\left(\frac{R_{2500}}{cm}\right) = 15.78 + 0.80 \log\left(\frac{M_{BH}}{10^9 M_\odot}\right) \quad (7)$$

leading size of NUV emission regions to be about  $48R_g$ . The estimated NUV emission regions have similar distances as the optical continuum emission regions in PG 1411+442 under the disk precession assumption, indicating that the disk precessions of emission regions are not preferred in PG 1411+442.

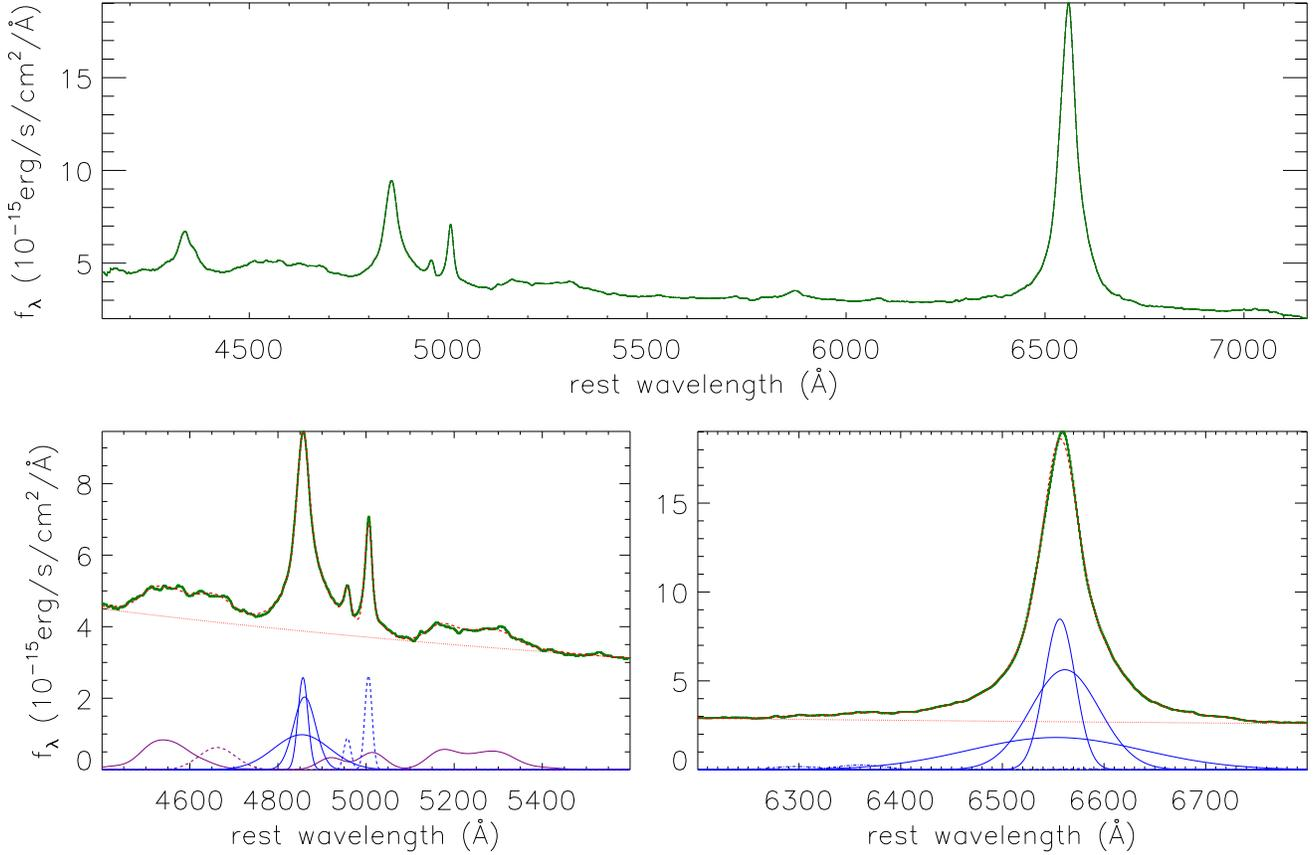


**Figure 7.** Top panel shows the average spectrum of PG 1411+422 collected from Kaspi et al. (2000). Bottom panels show the best fitting results (dashed red lines) to the emission lines (solid dark green lines) around H $\beta$  and around H $\alpha$ . In each bottom panel, dotted red line shows the determined power law continuum emissions, solid blue lines show the determined Balmer emission lines including three Gaussian components. In bottom left panel, solid purple line shows the determined optical Fe II emission lines, dashed purple line shows the determined broad He II component, dashed blue lines show the determined [O III] doublet.

Meanwhile, long-standing QPOs can be detected in blazars due to jet precessions as discussed in Sandrinelli et al. (2018); Bhatta (2019); Otero-Santos et al. (2020). PG 1411+442 is covered in Faint Images of the Radio Sky at Twenty-cm (Becker, White & Helfand 1995; Helfand et al. 2015) with peak flux about 1.61 mJy, leading to the corresponding radio loudness about 0.01, indicating PG 1411+442 as a radio quiet object. Therefore, jet precessions can be well ruled out in PG 1411+442.

We thirdly try to discuss spatial properties of the central BBH system through spectroscopic emission line features in PG 1411+442. Unfortunately, through the optical average spectrum in Kaspi et al. (2000) and the single-epoch spectrum in Boroson & Green (1992) of PG 1411+442, there are no unique features in broad Balmer lines probably related to the central BBH system, such as double-peaked features, very asymmetric features, etc., as the shown spectroscopic results in Fig. 7. Here, we do not show further discussions on our model functions including multiple Gaussian functions plus

optical Fe II template to describe the emission lines around H $\beta$  and around H $\alpha$  which is beyond the scope of the manuscript, detailed descriptions on our model functions can be found in our paper Zhang (2021b). Therefore, there are no further discussions on the probable BBH system through spectroscopic emission features of PG 1411+442. Moreover, as discussed in Bogdanovic et al. (2008); Shen & Loeb (2010); D’Orazio et al. (2015); Nguyen et al. (2020); Ji et al. (2021), BBHs can lead to variability of broad emission line profiles. However, considering variability of central ionization continuum emissions leading to deeper/shallower ionization boundaries in the BLRs (to change geometric structure of BLRs for broad line emissions), variability of broad emission line profiles can be well expected, not due to central BBHs but due to common intrinsic AGN variability, such as the known variability of broad emission lines of the reverberation mapped broad line AGN. Therefore, at present stage, we do not show further discussions on variability of spectroscopic emission features of PG 1411+442 probably related to BBH

system, due to loss of definite methods to determine effects of intrinsic AGN variability on variability of broad emission lines. However, the results in this manuscript provide clues to support indicators for BBHs by different line profiles in not only single-epoch spectrum but also in rms spectrum through multi-epoch spectra.

#### 4. SUMMARY AND CONCLUSIONS

Motivated by optical QPOs candidates expected in broad line AGN with very different line profiles of broad Balmer emission lines, the known reverberation mapped broad line AGN PG 1411+442 is selected as the subject of this manuscript, due to its very different dynamical properties of the varying components in the broad Balmer emission lines in its rms spectrum. Through the 18.8years-long light curves collected from the CSS, ASAS-SN and ZTF, stable 550days optical QPOs can be confirmed with confidence levels higher than  $5\sigma$  in PG 1411+442, through different methods/techniques. Furthermore, based on the CAR process, confidence level higher than  $3.5\sigma$  can be confirmed that the optical QPOs are not related to intrinsic AGN variability in PG 1411+442. The robust optical QPOs can be applied to support a BBH system candidate in the PG 1411+442. The results not only

provide clues to support that even central BBH system candidates expected in normal broad line AGN, the virial technique can also be efficiently applied to estimate central total BH masses, but also provide confident clues for searching optical QPOs among broad line AGN with very different line profiles of broad Balmer emission lines in the near future.

#### ACKNOWLEDGMENTS

Zhang gratefully acknowledge the anonymous referee for giving us constructive comments and suggestions to greatly improve our paper. Zhang gratefully acknowledges the kind grant support from NSFC-12173020 and NSFC-12373014. This paper has made use of the data from the ZTF <https://www.ztf.caltech.edu>, from ASAS-SN <https://www.astronomy.ohio-state.edu/asassn/index.shtml>, from CSS <https://catalina.lpl.arizona.edu/>. This research has made use of the NASA/IPAC Extragalactic Database (<http://ned.ipac.caltech.edu/classic/>) funded by the National Aeronautics and Space Administration and operated by the California Institute of Technology.

#### REFERENCES

- An, T.; Lu, X.; Wang, J., 2016, *A&A*, 585, 89
- Attard, K.; Gualandris, A.; Read, J. I.; Dehnen, W., 2024, *MNRAS* in press, arXiv:2402.10709
- Bogdanovic, T.; Smith, B. D.; Sigurdsson, S.; Eracleous, M., 2008, *ApJS*, 174, 455
- Becker, R. H., White, R. L., Helfand, D. J. 1995, *ApJ*, 450, 559
- Begelman, M. C., Blandford, R. D., Rees, M. J., 1980, *Natur*, 287, 307
- Bellm E. C., Kulkarni, S. R.; Barlow, T., et al., 2019, *PASP*, 131, 068003
- Bentz M. C., Denney, K. D.; Grier, C. J.; et al., 2013, *ApJ*, 767, 149
- Bhatta, G., 2019, *Universe Proceedings*, 17, 15, arXiv:1909.10268
- Bhattacharyya, J.; Ghosh, R.; Chatterjee, R.; Das, N., 2020, *ApJ*, 897, 25
- Boroson, T. A.; Green, R. F., 1992, *ApJS*, 80, 109
- Charisi, M.; Bartos, I.; Haiman, Z.; et al., 2016, *MNRAS*, 463, 2145
- Dekany, R.; Smith, R. M.; Riddle, R., et al., 2020, *PASP*, 132, 038001
- D’Orazio, D. J.; Haiman, Z.; Duffell, P.; Farris, B. D.; MacFadyen, A. I., 2015, *MNRAS*, 452, 2540
- Drake, A. J.; Djorgovski, S. G.; Mahabal, A., et al., 2009, *ApJ*, 696, 870
- Eracleous, M.; Livio M.; Halpern, J. P., 1995, *ApJ*, 438, 610
- Eracleous, M.; Boroson, T. A.; Halpern, J. P.; Liu, J., 2012, *ApJS*, 201, 23
- Foster, G., 1996, *AJ*, 112, 1709
- Fragione, G.; Grishin, E.; Leigh, N. W. C.; Perets, H. B.; Perna, R., 2019, *MNRAS*, 488, 47
- Graham, M. J.; Djorgovski, S. G.; Stern, D., et al., 2015a, *Natur*, 518, 74
- Graham, M. J.; Djorgovski, S. G.; Stern, D., et al., 2015, *MNRAS*, 453, 1562
- Green, J. E.; Ho, L. C., 2005, *ApJ*, 630, 122
- Gupta, A. C.; Tripathi, A.; Wiita, P. J.; et al., 2018, *A&A*, 616, 6
- Helfand, D. J.; White, R. L.; Becker, R. H., 2015, *ApJ*, 801, 26
- Ivezic, Z.; Connolly, A. J.; VanderPlas, J. T.; Gray, A., 2019, *Statistics, Data Mining, and Machine Learning in Astronomy: A Practical Python Guide for the Analysis of Survey Data*, ISBN: 9780691197050, Princeton University Press
- Ji, X.; Lu, Y.; Ge, J.; Yan, C.; Song, Z., 2021, *ApJ*, 910, 101
- Kaspi, S., Smith, P. S., Netzer, H., Maoz, D., Jannuzi, B. T., Giveon, U., 2000, *ApJ*, 533, 631
- Kasliwal, V. P.; Vogeley, M. S.; Richards, G. T., 2017, *MNRAS*, 470, 3027
- Kelly, B. C.; Bechtold, J.; Siemiginowska, A., 2009, *ApJ*, 698, 895
- Kelly, B. C.; Becker, A. C.; Sobolewska, M.; Siemiginowska, A.; Uttley, P., 2014, *ApJ*, 788, 33
- Kishore, S.; Gupta, A. C.; Wiita, P. G., 2024, *ApJ*, 960, 11

- Kochanek, C. S.; Shappee, B. J.; Stanek, K. Z.; et al., 2017, *PASP*, 129, 4502
- Kovacevic, A. B.; Popovic, L. C.; Simic, S.; Ilic, D., 2019, *ApJ*, 871, 32
- Kovacevic, A. B.; Yi, T.; Dai, X.; et al., 2020, *MNRAS*, 494, 4069
- Kozlowski, S.; Kochanek, C. S.; Udalski, A., et al., 2010, *ApJ*, 708, 927
- Kushwaha, P.; Sarkar, A.; Gupta, Alok C.; Tripathi, A.; Wiita, P. J., 2020, *MNRAS*, 499, 653
- Li, X.; Cai, Y.; Yang, H.; Luo, Y.; Yan, Y.; He, J.; Wang, L., 2021, *MNRAS*, 506, 2540
- Liao, W.; Chen, Y.; Liu, X.; et al., 2021, *MNRAS*, 500, 4025
- Liu, T.; Gezari, S.; Heinis, S., et al., 2015, *ApJL*, 803, L16
- Liu, T.; Gezari, S.; Miller M. C., 2018, *ApJL*, 859, L12
- Lomb, N. R., 1976, *Ap&SS*, 39, 447
- MacLeod, C. L.; Ivezić, Z.; Kochanek, C. S., et al., 2010, *ApJ*, 721, 1014
- Mannerkoski, M.; Johansson, P. H.; Rantala, A.; Naab, T.; Liao, S.; Rawlings, A., 2022, *ApJ*, 929, 167
- Markwardt, C. B., 2009, *ASPC*, 411, 251
- Mayer, L.; Kazantzidis, S.; Escala, A.; Callegari, S., 2010, *Natur*, 466, 1082
- Morgan, C. W.; Kochanek, C. S.; Morgan, N. D.; Falco, E. E., 2010, *ApJ*, 712, 1129
- Moreno, J.; Vogeley, M. S.; Richards, G. T.; Yu, W., 2019, *PASP*, 131, 063001
- Nguyen, K.; Bogdanovic, T.; Runnoe, J. C.; Eracleous, M.; Sigurdsson, S.; Boroson, T., 2020, *ApJ*, 894, 105
- Otero-Santos, J.; Acosta-Pulido, J. A.; Becerra Gonzalez, J.; et al., 2020, *MNRAS*, 492, 5524
- Peterson B. M.; Ferrarese, L.; Gilbert, K. M., et al., 2004, *ApJ*, 613, 682
- Rees, M. J., 1984, *ARA&A*, 22, 471
- Sandrinelli, A.; Covino, S.; Treves, A.; et al., 2018, *A&A*, 615, 118
- Scargle, J. D., 1982, *ApJ*, 263, 835
- Serafinelli, R.; Severgnini, P.; Braito, V., et al., 2020, *ApJ*, 902, 10
- Shappee, B. J.; Prieto, J. L.; Grupe, D.; et al., 2014, *ApJ*, 788, 48
- Shen, Y.; Loeb, A., 2010, *ApJ*, 725, 249
- Silk, J.; Rees, M. J., 1998, *A&A*, 331, L1
- Storchi-Bergmann, T.; Nemmen da Silva, R.; Eracleous, M., et al., 2003, *ApJ*, 598, 956
- Tarnopolski, M.; Zywuca, N.; Marchenko, V.; Pascual-Granado, J., 2020, *ApJS*, 250, 1
- VanderPlas, J. T., 2018, *ApJS*, 236, 16
- Vaughan, S.; Uttley, P.; Markowitz, A. G.; et al., 2016, *MNRAS*, 461, 3145
- Wang, J.; Songsheng, Y.; Li, Y.; Du, P., 2023, *MNRAS*, 518, 3397
- Yu, W.; Richards, G. T.; Vogeley, M. S.; Moreno, J.; Graham, M. J., 2022, *ApJ*, 936, 132
- Zechmeister, M.; Kurster, M., 2009, *A&A*, 496, 577
- Zhang, X. G., 2021b, *ApJ*, 909, 16, arXiv:2101.02465
- Zhang, X. G., 2021, *MNRAS*, 507, 5205, arXiv:2108.09714
- Zhang, X. G., 2022a, *MNRAS*, 512, 1003, arXiv:2202.11995
- Zhang, X. G., 2022b, *MNRAS*, 516, 3650, arXiv:2209.01923
- Zhang, X. G., 2023a, *MNRAS*, 526, 1588, arXiv:2309.08078
- Zhang, X. G., 2023b, *MNRAS*, 525, 335, arXiv:2307.09041
- Zheng, Z.; Butler, N. R.; Shen, Y.; et al., 2016, *ApJ*, 827, 56